ARTICLE NO. 78-1240

Performance of a Ring Laser Strapdown Attitude and Heading Reference for Aircraft

Carlo San Giovanni Jr.*
Sperry Gyroscope, Sperry Rand Corporation, Great Neck, N.Y.

This paper describes an accuracy performance analysis of a generic ring laser strapdown attitude and heading reference system (AHRS) operating in an aircraft environment. The system configuration includes magnetic heading and airspeed sensors to provide required heading and velocity reference information, and a fifteen-state Kalman filter to process the measurement data. Covariance analysis results are presented to indicate the relationship of system accuracy performance to gyro drift and to wind characteristics. For example, these results show that a pitch/roll accuracy of approximately 4 arc-min (rms) can be provided using ring laser gyros with a 0.15 deg/h$^{1/2}$ white noise drift. Selection of gyros with white noise drift of 0.05 deg/h$^{1/2}$ will reduce these errors to 2.5 arc-min (rms) per axis. These gyro drift characteristics are well within the range of current ring laser gyro designs. The study also showed that the magnitude of wind variations in the 4.5-7 rad/h frequency region is an important feature of this error source. It is concluded that state-of-the-art ring laser strapdown systems are fully compatible with accuracy requirements of an aircraft AHRS.

Introduction

THE practical implementation of a strapdown inertial system requires a high-speed computational capability and inertial sensors with a wide dynamic range. Given these elements, such systems potentially provide significant advantages in cost, reliability, and maintainability relative to gimballed configurations. Note also that strapdown systems directly provide body rates and accelerations; these strapdown system outputs can be used for flight control and/or fire control purposes, thus eliminating the need for separate sensors.

The computational and sensor requirements of strapdown systems derive from the need to measure rates and accelerations in a vehicle frame, and to transform the acceleration data into an earth-fixed frame. The transformation operation implies a high-speed update of the direction cosine matrix relating the vehicle and earth-fixed frames. The associated computational burden is well within the capabilities of the state-of-the-art digital computer. Acceleration measurement requirements are also fully met by state-of-the-art units.

Both conventional (spinning wheel) and unconventional gyros have been used in strapdown systems. The ring laser is an unconventional gyro which is particularly well matched to the strapdown environment. The theory of operation of this device has been detailed in the literature.[1,2] Briefly, the ring laser gyro consists of a ring-type optical cavity and a gain medium. Laser action produces oppositely directed traveling waves which traverse the same closed optical path. In the absence of rotation of the cavity, these traveling waves have the same frequency of oscillation. Rotation (with respect to inertial space) about an axis normal to the lasing plane changes the oscillation frequency of each wave. Measurement of the difference (beat) frequency between the waves provides a precise indication of the input angular rotation rate.

Ring laser gyros have the capability for accurately measuring rates over a wide dynamic range, and they inherently provide a direct digital output. The absence of moving parts implies high reliability and low cost. In addition, ring laser gyro drift characteristics are essentially independent of the acceleration environment. These favorable circumstances have led to development of several ring laser strapdown systems.[3-8] Based on their demonstrated and potential cost and performance capabilities, it is clear that ring laser strapdown systems qualify as prime candidates for a broad spectrum of applications.

The aircraft attitude and heading reference system (AHRS) discussed in this paper represents a particular potential application for ring laser strapdown systems in which cost, reliability, and maintainability are paramount considerations. It is, then, of special interest to establish the performance requirements imposed by a high-accuracy AHRS on the ring laser inertial sensors. Covariance analysis techniques are used to provide the desired information. Since the use of an optimal filter is assumed, the results comprise a lower bound on system errors. The analysis primarily pertains to constant altitude flight conditions; the influence of some vehicle maneuvers is indicated.

The analyses described in the paper specifically apply to a ring laser strapdown system. In particular, the strapdown concept implies that gyros and accelerometers (and, therefore, gyro and accelerometer errors) are fixed to the body axes. In contrast to a gimballed configuration, error propagation characteristics of a strapdown system are directly dependent on vehicle maneuvers; this condition is included in the mathematical model of the inertial plant used in the analyses. Further, the assumed flight conditions include two 2 g 90-deg turns to illustrate the influence of vehicle maneuvers on strapdown system attitude accuracy performance. The use of ring laser gyros rather than conventional (spinning wheel) gyros is implicit in the model used to represent gyro drift. There are at least two distinguishing features of a ring laser gyro which are pertinent. 1) The drift of the ring laser gyro is dominated by uncorrelated (white) noise. Such components are quite small in the case of spinning wheel gyros; their major drift components usually involve correlation times in the order of 1 h (and greater). 2) Ring laser gyro drift is independent of the acceleration environment. In contrast, accelerations associated with vehicle maneuvers influence drift of spinning wheel gyros through both g-sensitive (mass unbalance) and g^2-sensitive (anisoelastic) terms.

Presented as Paper 78-1240 at the AIAA Guidance and Control Conference, Palo Alto, Calif., Aug. 7-9, 1978; submitted Aug. 16, 1978; revision received Jan. 16, 1979.

Index categories: Guidance and Control; Navigation, Communication, and Traffic Control; Sensor Systems.

*Research Section Head, Advanced Navigation Systems. Member AIAA.

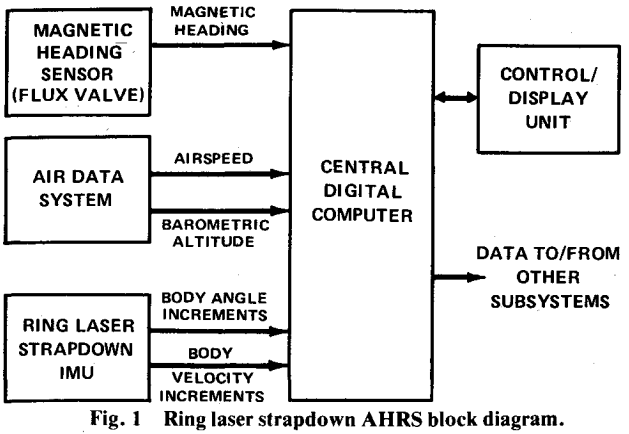

Fig. 1 Ring laser strapdown AHRS block diagram.

A general AHRS configuration is briefly described in the next section; it provides the basis for the analysis. This is followed by the details of the associated math and error model, and of the model parameters. The technique used to conduct the analysis, and the assumed operating conditions are then indicated. Results, primarily consisting of a time history of rms attitude errors under various conditions and assumptions, are presented, and pertinent conclusions are stated.

System Configuration

An attitude and heading reference system implies the availability of suitable heading and velocity reference information. For the aircraft systems under consideration, magnetic heading data is assumed to be available for use as the heading reference; airspeed, as provided by the air data system, comprises the velocity reference. A generic AHRS configuration is shown in Fig. 1; that block diagram is intended to be illustrative rather than definitive. Many variants involving the organization of equipment and computational functions are possible.

As indicated in Fig. 1, the strapdown inertial measurement unit (IMU) provides body angle increments (as measured by three ring laser gyros) and body velocity increments (as measured by three accelerometers) to a central digital computer. This inertially derived information is processed via an appropriate set of strapdown computational algorithms and then combined with reference data in a Kalman filter to generate optimal estimates of aircraft attitude/heading. Other navigational data (velocity/position) as well as body rates and accelerations are also available for use.

In Fig. 1, magnetic heading reference information is provided from a flux value. Corrections for magnetic variation can be considered to be generated in the computer via an appropriate position-dependent model; as an alternate, magnetic variation could be input via the control/display unit (CDU). The air data system provides both airspeed and barometric altitude. Airspeed, appropriately resolved, is used as the horizontal velocity reference; barometric altitude (or radar altimeter data, if available) is used as the reference for the vertical velocity computation.

The Kalman filter algorithm is assumed to be implemented in the digital computer. For purposes of this paper, this filter operates only on the difference between 1) inertial and reference heading, and 2) inertial horizontal velocities and the corresponding horizontal components of the airspeed reference. With some increase in complexity, the difference between inertial and barometric altitude also could have been included in the structure of the Kalman filter.[9] The filter outputs constitute estimates of the modelled states and would be used to correct the corresponding system error sources and outputs.

Estimates of tilt errors are developed in the Kalman filter primarily through use of information contained in the velocity differences. In general, the velocity differences may be represented as the combination of inertial system velocity error (the error in inertially-derived ground velocity) and of reference error (the error in the reference indication of ground velocity). In this case, the velocity reference is airspeed, so that winds comprise the major reference error. The inertial system velocity error in each axis includes a component reflecting the integral of (uncorrelated) attitude errors, i.e., $\int(g\cdot\delta\theta+\xi_A)\,dt$ where g designates gravity, $\delta\theta$ is the tilt, and ξ_A represents acceleration errors. (Note that in a strapdown system, a/c turns will decouple previously correlated tilts and accelerometer biases, thus leading to "observability" of these states.) In the ideal situation, reference errors are negligible, and the velocity differences provide accurate "observations" of the tilts, and of casual inertial system error sources. For example, this condition would apply during stationary ground alignment, or if an accurate measure of groundspeed (e.g., doppler radar) were available as an in-air reference. In this system, however, reference velocity error (wind) is a significant error source, and certain of its characteristics will exert an important influence on tilt estimation accuracy. The effect generally depends on the degree of overlap between the frequency spectra of the tilts and of winds, and also on the relative magnitude of these errors. Use of Schuler tuning causes the spectra of tilts due to gyro drift/acceleration errors to peak in the vicinity of 4.5 rad/h. Wind variations in this same frequency region would then cause the velocity differences to provide a somewhat ambiguous indication of attitude errors. Therefore, the magnitude of the wind power spectral density in the region near Schuler frequency can be expected to limit tilt estimation accuracy. Use of a Kalman filter, structured to include all important error propagation and error source properties, ensures that any such lower bound will be reached, i.e., that "optimal" estimates of all the modeled states, including tilts, will be generated.

Mathematical and Error Model

Conduct of an accuracy analysis requires definition of a mathematical model of the system and of the pertinent characteristics of the error sources. The mathematical model describes the manner in which the various error sources propagate into errors in the system outputs. Use of a state space format is particularly convenient and appropriate. Assuming that the system is linear (or linearized), the math model can be represented by the following vector equations:

State Space Equation:

$$\dot{X}(t)=AX(t)+\eta(t) \tag{1}$$

Measurement Equation:

$$Z(t)=HX(t)+\nu(t) \tag{2}$$

where X is the state vector (dimension n), Z is the observation vector (dim r), A is the $n\times n$ system matrix, H is the $r\times n$ measurement matrix, η is the white plant noise vector (dim n), and ν is the white measurement noise vector (dim r). The state vector, X, can be partitioned into three components: 1) those states describing the unforced dynamical behavior of the unaugmented plant (in this case, the plant comprises the Schuler loop and earth loop dynamics); 2) the states describing the dynamical characteristics of the plant error sources (viz. gyro drift and acceleration errors); and 3) the states describing the errors in the references (i.e., the errors in the heading and velocity reference information). For purposes of this analysis, a fifteen-state system was formulated to represent the dynamical characteristics of the plant and of the error sources. The states include inertial velocity errors (2), attitude errors (2), inertial heading error (1), latitude error (1), gyro drifts (3), accelerometer errors (2), magnetic heading reference error (1), winds (2), and airspeed bias error (1).

Z, the observation vector, characterizes the "noisy" measurements of linear combinations of the states. In this

1. $\dot{\delta V}x = -2(\Omega + \dot{\lambda}) \sin L\ [\delta Vy] + g\ [\delta\theta y] + (Ay - Vx \sin L\ (2\Omega + \dot{\lambda})\ [\delta\theta z] - Vy\ (2\Omega \cos L + \dot{\lambda} \sec L)\ [\delta L] + \xi_{AX} + \eta_{AWX}$

2. $\dot{\delta V}y = (2\Omega + \dot{\lambda}) \sin L\ [\delta Vx] + \frac{Vx}{R} \tan L\ [\delta Vy] - g\ [\delta\theta x] - (Ax + Vy \sin L\ (2\Omega + \dot{\lambda}))\ [\delta\theta x] + Vx\ (2\Omega \cos L + \dot{\lambda} \sec L)\ [\delta L] + \xi_{AY} + \eta_{AWY}$

3. $\dot{\delta\theta}x = \frac{1}{R} [\delta Vy] - (\Omega + \dot{\lambda}) \sin L\ [\delta\theta y] + \frac{Vx}{R} [\delta\theta z] - \Omega \sin L\ [\delta L] + \xi_{GX} + \eta_{GWX}$

4. $\dot{\delta\theta}y = -\frac{1}{R} [\delta Vx] + (\Omega + \dot{\lambda}) \sin L\ [\delta\theta x] + (\Omega + \dot{\lambda}) \cos L\ [\delta\theta z] + \xi_{GY} + \eta_{GWY}$

5. $\dot{\delta\theta}z = -\frac{\tan L}{R} [\delta Vy] - \frac{Vx}{R} [\delta\theta x] - (\Omega + \dot{\lambda}) \cos L\ [\delta\theta y] - (\Omega \cos L + \dot{\lambda} \sec L)\ [\delta L] + \xi_{GZ} + \eta_{GWZ}$

6. $\dot{\delta L} = \frac{1}{R} [\delta Vx]$

$\delta Vx, y$ N/S, E/W VELOCITY ERRORS

$\delta\theta x, y$ TILT ABOUT NORTH (X), EAST (Y) AXES

$\delta\theta z$ HEADING ERROR

δL LATITUDE ERROR

$R; \Omega$ EARTH'S RADIUS; EARTH RATE

$L; \dot{\lambda}$ VEHICLE LATITUDE; LONGITUDE RATE

$\xi_{AX, AY}$ N/S, E/W COMPONENTS* OF ACCEL. ERRORS

$\xi_{GX, GY, GZ}$ N/S, E/W, VERT. COMPONENTS* OF GYRO ERROR

$\eta_{AWX, AWY}$ N/S, E/W, COMPONENTS OF "WHITE" ACCEL. ERROR

$\eta_{GWX, GWY, GWZ}$ N/S, E/W, VERT. COMPONENTS OF "WHITE" GYRO DRIFT

g GRAVITY

*COMPONENTS ARE THE PROJECTIONS OF ERRORS IN BODY AXES ONTO THE GEOGRAPHIC FRAME USING ELEMENTS OF THE DIRECTION COSINE MATRIX

Fig. 2 Inertial error equations.

Table 1 Gyro drift model parameters

Gyro model	Bias drift, deg/h	White noise, deg/h$^{1/2}$	Random walk, (deg/h)/h$^{1/2}$
A	1.0	0.010	0.150
B	1.0	0.050	0.150
C	2.0	0.150	0.150
D	5.0	0.300	0.150

case, Z is the error vector associated with the airspeed measurements of inertial horizontal velocities, and with the magnetic heading measurements of inertial heading.

Inertial System Plant Equations

The implementation of a strapdown inertial system requires the use of three gyros and three accelerometers to completely measure vehicle motions. This implies the need to mechanize a vertical velocity loop and to provide an appropriate altitude reference. A complete description of the inertial plant dynamics would then require a model of the vertical axis as well as of the horizontal axes. In general, the vertical axis error equations are not strongly coupled to the error equations for the horizontal axes. In addition, the aircraft trajectories used in this analysis assume constant altitude operations, which further weakens any crosscoupling effects. On this basis, the error equations for the inertial plant were restricted to a two-axis model describing behavior in the horizontal axes. The equations are shown in Fig. 2. Derivations are available in the literature.[10] Six states are involved, and they are defined in a geographic frame. The states are N/S and E/W velocity errors (2), tilts about the N/S and E/W axes (2), inertial heading error (1), and latitude error (1). The input axes of the strapped-down gyros and accelerometers are assumed to be aligned with the principal axes of the aircraft. Gyro and accelerometer errors are mapped into the geographic frame using appropriate elements of the direction cosine matrix. These elements generally consist of functions of aircraft attitude/heading. However, for the assumed conditions of this study, the particular direction cosine matrix elements comprise trigonometric functions of aircraft heading.

Gryo Drift Errors

A complete description of those errors appearing as gyro drift in a ring laser strapdown system could involve a large number of states. For example, a model which includes a bias state, scale factor error, and three misalignments per gyro would require a total of 12 states for the three gyros. For purposes of this analysis, the drift behavior of the ring laser gyro over the time periods of interest has been modelled as the combination of a random bias (turn-on to turn-on repeatability), a white random process, and a random walk process. This representation requires one state for each of the three gyros (total of three states).

The effect of scale factor errors, misalignments, etc. may be considered to be subsumed in the white and random walk components of this model. In particular, the extent of gyro drift associated with such effects depends not only on the sensor error parameters but also on the magnitude of vehicle rates. The assumption that the frequency of occurrence and the magnitude of vehicle rates is random provides a general rationale for characterizing the resultant drift as a random process. The use of the random walk component is only considered valid over restricted time periods. The white, or wideband, drift constitutes the dominant random self-drift component in the ring laser; this has been shown both theoretically and through various analyses of test stand data.[3-6,11]

The white noise components of gyro drift are used to form the white plant noise elements for the attitude/heading errors (states, 3, 4, 5) in the equations of Fig. 2. For conditions of this analysis, the covariance matrix of the white input noise for these states (which represent errors in earth-fixed axes) is diagonal and is independent of the direction cosine matrix. This follows from the assumption that the white drift in each gyro axis is independent and has identical variance. The form of the state equation for the bias and random walk drift is

$$\dot{\epsilon}_{Gi} = \eta_{Gi} \tag{3}$$

($i = a, b, c$; these designate gyro axes corresponding to body axes)

The gyro drift model parameters were varied as part of this analysis. The specific parameters used are listed in Table 1.

Acceleration Errors

A complete description of acceleration errors would include accelerometer turn-on bias, bias stability, scale-factor errors, misalignments, nonlinearities, and external effects due to vertical deflections and gravity anomalies. For this analysis, acceleration errors were modeled as the combination of a turn-on bias, white noise, and random walk with rms values of 112 μg, 2.0 kt/h$^{1/2}$, and 35 μ g/h$^{1/2}$, respectively. The form of the model is similar to that used for the gyros; only one state is required in each axis (total of two states). The selected parameters generally represent state-of-the-art accelerometers. The indicated random walk magnitude is particularly conservative and is only considered valid over restricted time periods.

Measurement Equations

As previously noted, magnetic heading and horizontal velocity measurements are used in the postulated Kalman

filter. The measurements describe the difference between inertially derived and available reference data. They can be represented as follows:

$$Z_1 = \psi_{MR} - \psi_I \quad \text{heading difference} \quad (4a)$$

$$Z_2 = V_{GXI} - V_{ASR} \cdot x_I \quad \text{N/S velocity difference} \quad (4b)$$

$$Z_3 = V_{GYI} - V_{ASR} \cdot y_I \quad \text{E/W velocity difference} \quad (4c)$$

where ψ_I, ψ_{MR} are inertially derived and (magnetic) reference heading, respectively; V_{GXI}, V_{GYI} are inertially derived north and east components of groundspeed, respectively; V_{ASR} is the reference (measured) airspeed; x_I, y_I are unit vectors directed along inertially indicated north and east axes, respectively; and $V_{ASR} \cdot x_I$ is the vector dot product, designating the computed projection of measured airspeed along the inertially indicated north axis. For the simplified conditions of this analysis

$$V_{ASR} \cdot x_I = V_{ASR} \cos\psi_I \quad (5a)$$

$$V_{ASR} \cdot y_I = V_{ASR} \sin\psi_I \quad (5b)$$

Equation (4a) represents the difference between inertially derived heading and (compensated) flux value data. This difference includes inertial heading error as well as errors in the reference heading. The velocity differences (Eqs. 4a and 4b) represent a comparison between inertially derived groundspeed and measured airspeed. Winds comprise a major element in these difference equations. The velocity differences also include inertial system velocity errors (which reflect errors in inertially derived attitude, i.e., the desired information) and airspeed sensor errors. Explicit formulation of the measurement equations in terms of these various errors is shown below.

The ground velocity vector and the heading of the aircraft can be expressed as

$$V_G = V_{AS} + W + v_W + \epsilon_{VAS} \quad (6a)$$

$$\psi = \psi_{MR} - \epsilon_{HR} - \nu_{HR} \quad (6b)$$

where

V_G = true groundspeed vector
V_{AS} = true airspeed vector
W = (low-frequency) wind vector
v_W = high-frequency components in measured airspeed (gusts)
ϵ_{VAS} = bias in measured airspeed
ψ = true aircraft heading
ϵ_{HR} = correlated error component in measured heading (after compensation for magnetic variation and flux value instrument errors)
ν_{HR} = white error component of measured heading

The above expressions can be used to reformulate the measurement equations as a linear combination of the modeled error states:

$$Z_1 = [\delta\theta_Z] + [\epsilon_{HR}] + \nu_{HR} \quad (7a)$$

$$Z_2 = [\delta V_X] + [W_X] - [\delta\theta_Z] V_{AS} \sin\psi - [\epsilon_{VAS}] \cos\psi + \nu_{WX} \quad (7b)$$

$$Z_3 = [\delta V_Y] + [W_Y] + [\delta\theta_Z] V_{AS} \cos\psi - [\epsilon_{VAS}] \sin\psi + \nu_{WY} \quad (7c)$$

where

W_x, W_y = components of W in the N/S, E/W directions

Table 2 (Correlated) wind model parameters

Wind model designation	Rms magnitude per axis, kt	Corr. time, h	Equiv.[a] corr. distance, n. mi.
I	28.0	2.5	1250
II	28.0	6.0	3000
III	71.0	20.0	10,000
IV	28.0	0.2	100
V	56.0	6.0	3000
VI	56.0	0.2	100
VII	23.0	0.05	25

[a] At an airspeed of 500 knots.

ν_{WX}, ν_{WY} = components of ν_W in the N/S, E/W directions

In formulating the velocity measurement equations, it is assumed either that the transverse velocity of the aircraft is zero, or that an appropriate transverse velocity reference has been computed.

Equation (7) describes the measurements in the form prescribed by Eq. (2). The terms in brackets are elements of the state vector, and their coefficients define the measurement matrix. It is noted that the use of Eq. (7) implies that appropriate models be included for errors in the reference data, i.e., magnetic heading reference errors, airspeed bias error, and winds. The models used for these quantities are discussed in the following paragraphs.

Magnetic Heading Reference Errors

The error in the magnetic reference was modeled as the combination of a zero-mean exponentially correlated process (standard deviation of 1 deg and a nominal correlation time of 0.5 h) and a white noise component (rms value of 15 arc-min). This model represents both uncompensated magnetic field fluctuations and flux value errors[12] over the time period and aircraft speeds of interest. One state is required to represent the exponentially correlated component. The form of the state equation is

$$\dot{X}_i = -1/\tau_i * X_i + \eta_i \quad (8)$$

where X_i represents the error state, τ_i is the corresponding correlation time, and η_i is the white input noise. If the input noise is Gaussian, then X_i is a first order Markov process.

Airspeed Bias Error

The error in indicated airspeed was modeled as a bias; one state is required for this representation. Analyses were conducted using an rms value for this state of 5 kt. This is considered a conservative measure of the combined effects of calibration error, scale factor, and linearity errors, etc.

Wind Model

N/S and E/W winds were assumed independent, and each was modeled as the combination of white noise (representing gusts) and a zero-mean exponentially correlated component (representing the low-frequency wind structure). This involved the use of one state per axis (total of two states); the form of the state equations is identical to that of Eq. (8).

There is substantial variation in the wind models which have appeared in related literature[12-15]; the use of engineering judgement to augment the sketchy available information is often cited. The models used in the literature include 1) a constant wind, plus gusts with an rms magnitude of 1 kt and correlation time of 2 s, 2) independent exponentially correlated N/S, E/W winds with rms value of 40 kt/axis and 10 min correlation time; aircraft speed is 500-600 kt, 3) similar to the model in 2) but a correlation distance of 50 n. mi., and

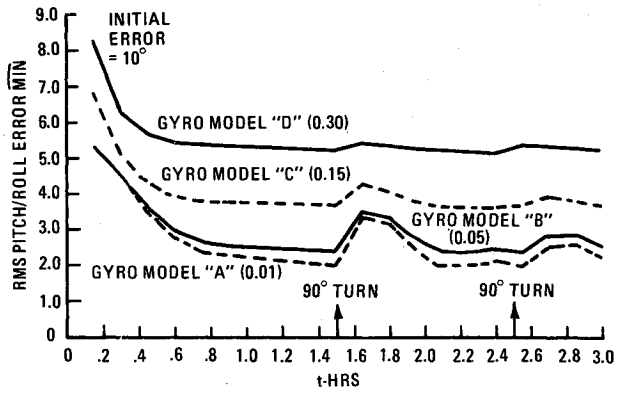

Fig. 3 Gyro model effects: wind model I.

4) the combination of a mean wind, a random walk component with magnitude of 25 kt/h$^{1/2}$, and gusts with rms value of 45 kt with one second correlation time.

Because of the lack of a standard wind model, the parameters used in this analysis were varied over a relatively wide range. The baseline wind model was obtained from information provided in Ref. 16. A normalized correlation function for winds is stated in that reference as

$$R(d)/\sigma^2 = 1.45\exp(-|d|/960) - 0.45\exp(-|d|/360) \quad (9)$$

where d is in n. mi. and $\sigma = 38.6$ kt. An adequate single exponential approximation was developed for use in the analysis,

$$R(d)/\sigma^2 = \exp(|d|/1250) \quad (10)$$

The wind model parameters used in the analysis to represent the low-frequency wind structure are shown in Table 2. Wind model I designates the baseline wind model. The other models were used to examine the influence of changes in the correlation time and in the rms magnitude of winds. Wind model III is essentially a random walk process over the 3-4 h flight times of interest. The equivalent random walk magnitude is approximately 23 kt/h$^{1/2}$.

The primary wind gust model used in the analyses comprised a white process with rms magnitude of 6 kt. Information in the literature indicates that reasonable values for rms gusts are in the range of 3-7 fps with a scale of 1000 ft (1.2 s correlation time at 500 kt airspeed). However, those values apply primarily to low altitude operations; rms gust magnitude generally increases with mean wind velocity at the operating altitudes of interest. The use of a 10.8 s iteration time in the analyses justifies the use of a white process to approximate the 1.2 s correlation times associated with gusts at the aircraft speeds of interest.

Analysis Approach

A generalized error analysis computer program was used to generate the results presented in this paper. This computer program assumes that the Kalman algorithm is used to process the available measurement data and develop estimates of the modeled system states. The covariance matrix of estimation errors is generated based on the assumption that the system is Gauss-Markov (linear system driven by white Gaussian noise), and that the error models used to structure the Kalman filter match the real world. For these conditions, the computed covariance matrix provides a lower bound on system errors.

The basic information required to conduct the error analysis has been detailed in the previous section of this paper. A fifteen-state model of the augmented plant and a measurement matrix of rank 3 was defined.

The square root of the diagonal elements in the computed covariance matrix represents the standard deviation of the estimation errors; this is the primary accuracy information presented in the sequel.

Conditions of Analysis

The analysis conditions included a constant altitude flight for 3 h at 500 kt airspeed. Operating latitude was 45°N, and initial heading (θ_{HO}) was 45 deg. Two 90 deg turns were assumed to occur, at approximately 1.5 h and at 2.25 h; turn acceleration was approximately 2 g.

The iteration interval selected for the Kalman filter was 10.8 s; this also defines the time between assumed measurements of magnetic heading and airspeed.

The conditions used generally imply in-air erection of the system.

Presentation of Results

The primary results of the paper are given in Figs. 3-9. These figures generally comprise plots of the rms error in a particular state vs time.

Figure 3 presents a time history of rms pitch/roll errors with the baseline wind model I. Performance with several of the gyro drift models is shown; some of the results are summarized in Table 3.

Initial rms tilts of 10 deg/axis were used in the analysis. Figure 3 shows, for example, that with gyro model C the system provides an rms pitch/roll accuracy of 6.2 arc-min within 12 min of time, and a steady-state accuracy of 3.7 arc-min/axis. Following alignment, the modeled error states, with the exception of latitude error, reached a statistical equilibrium. This steady-state condition implies a strong correlation between many of the error states. Among the more obvious is the correlation of inertial velocity errors with the combined (resolved) wind and airspeed bias error, the inertial heading error with the magnetic heading reference error, and tilt errors with accelerometer biases. Aircraft turns generally assist, and in some cases are vital to, the calibration of many of these states. This is particularly the case with a strapdown system, since the inertial error sources rotate with the aircraft axes while previously correlated output errors remain spatially fixed. For example, errors in computed earth rate and in attitude are spatially fixed while casual error sources such as gyro drift and accelerometer errors rotate with the aircraft. This also applies to airspeed reference errors since winds are assumed to be spatially fixed while airspeed bias error is fixed to the aircraft axes. The occurrence of turns is then expected to result in transient errors due to decorrelation effects. However, since information about the

Table 3 Rms pitch/roll errors with baseline wind model I

Gyro model	White noise, deg/h$^{1/2}$	Rms pitch/roll error, arc-min: At $t = 0.2$ h	Steady state	Peak; first 90 deg turn	Peak; second 90 deg turn
A	0.01	5.1	2.0	3.4	2.6
B	0.05	5.1	2.4	3.5	2.6
C	0.15	6.2	3.7	4.3	3.9
D	0.30	7.6	5.2	5.4	5.3

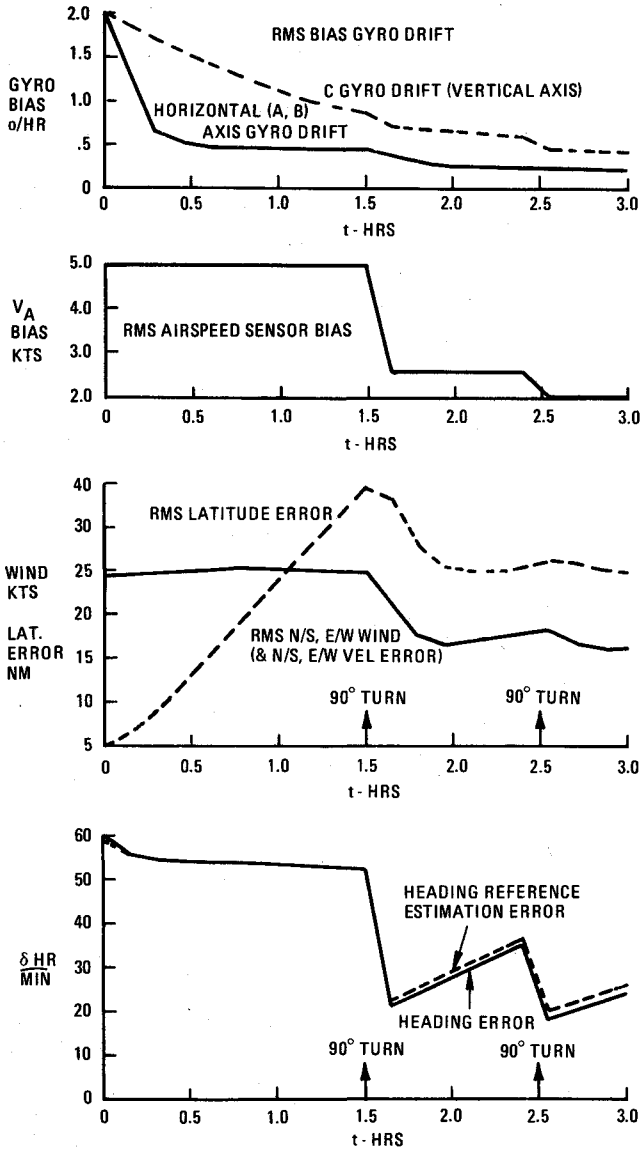

Fig. 4 Rms estimation errors: gyro model C, wind model I.

effect of the turn on system errors is included in the Kalman filter structure, the resultant velocity and heading errors generally are used by the filter to generate improved estimates of the error sources. Successive turns can usually be expected to result in successively lower transient errors and in correspondingly lesser improvements in error source calibration. This statement assumes that the time duration between turns is sufficiently long to permit enough measurements for effective calibration, but is also shorter than the correlation time of the estimated states (so that any previous calibration has not significantly degraded). Figure 3 and Table 3 demonstrate the effect of successive turns. It is noted that use of specific models for scale factor errors and misalignments would generally cause some increase in transients.

Figure 4 provides a time history of the estimation errors in gyro drifts, airspeed bias error, winds and inertial velocity errors, latitude error, and heading/heading reference error. The data applies for gyro model C with the baseline wind model I. Figure 4 shows that bias drift is calibrated to 0.21 deg/h in each of the horizontal (*a, b*) axes, and to 0.41 deg/h in the vertical (*c*) axis. The major portion of the gyro bias calibration is accomplished prior to occurrence of the turns; however, the turns favorably influence gyro bias estimation especially in the case of the *c* gyro. In contrast, calibration of airspeed sensor bias is totally dependent on the occurrence of

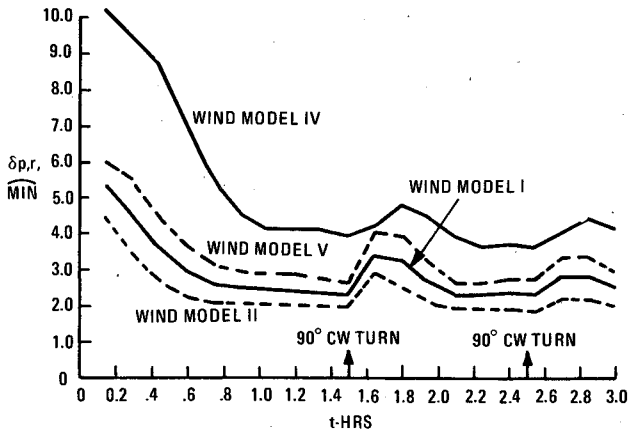

Fig. 5 Wind model effects: gyro model B.

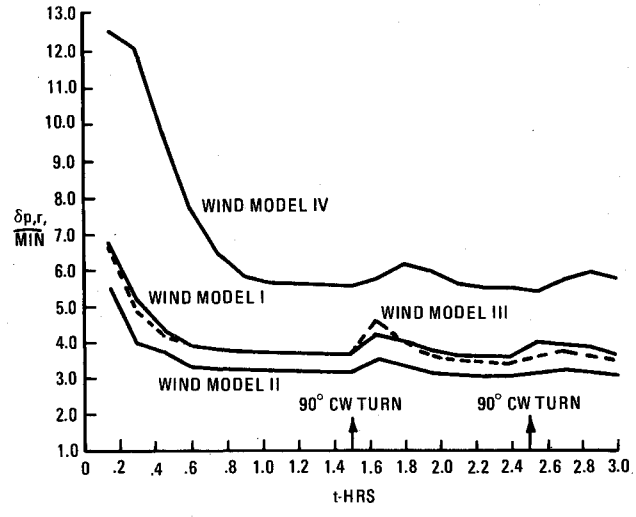

Fig. 6 Wind model effects: gyro model C.

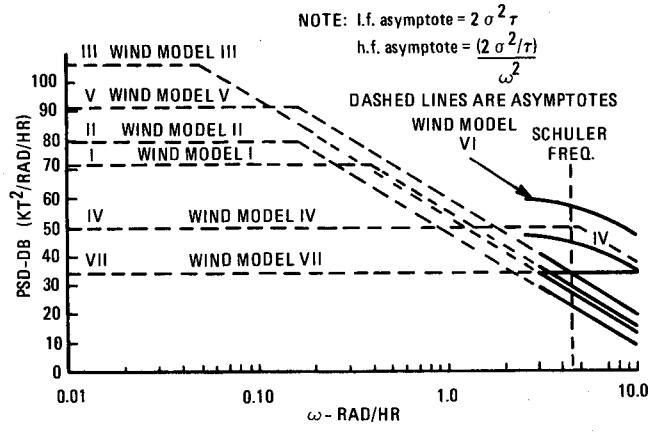

Fig. 7 Wind model power spectral density.

turns. The data indicates that the execution of a few 90 deg turns calibrates this state to approximately 2 kt. The calibration of N/S, E/W winds is also dependent on the occurrence of aircraft turns; the winds in each axis are estimated, after the turns, to an rms value of approximately 16 kt. Because of the dynamics of the assumed wind structure (2.5 h correlation time), the calibration of winds following each turn is temporary. The plot shows a gradual degradation in wind calibration following the first turn, and a recalibration after the second turn. It is noted that the plot of N/S, E/W winds is also essentially a plot of N/S, E/W velocity errors. Latitude error behavior is also indicated in

Table 4 Rms pitch/roll errors

Wind model			Steady-state pitch/roll error, arc-min		
No.	Knots	Hours	Gyro model A	Gyro model B	Gyro model C
VI	56.0	0.20	5.5	6.0	7.6
IV	28.0	0.20	3.2	3.7	5.4
VII	23.0	0.05	–	2.6	4.5
I	28.0	2.5	2.0	2.4	3.6
II	28.0	6.0	1.6	1.9	3.1
V	56.0	6.0	2.2	2.7	4.0
III	71.0	20.0	–	–	3.5

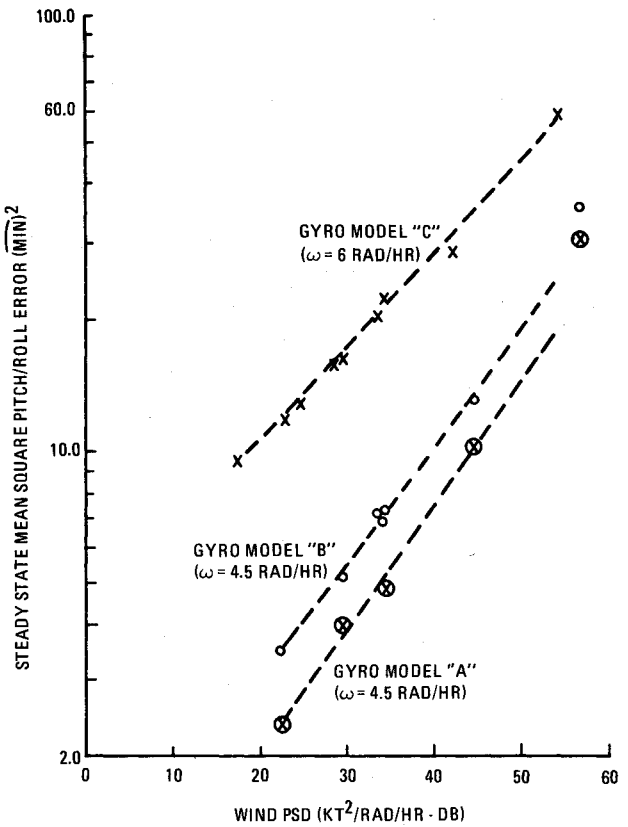

Fig. 8 Mean square ss pitch/roll error vs wind psd at specific frequency.

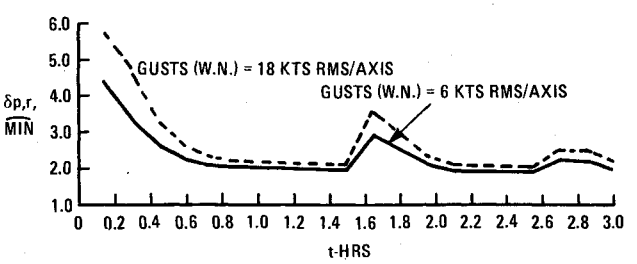

Fig. 9 Effect of gust model: gyro model B.

Fig. 4. The plot indicates that the occurrence of turns can bound latitude error in this case to about 25 n. mi.; calibration is associated with the influence of latitude error on horizontal earth rate ($\Omega \sin L \cdot \Delta L$).

Figure 4 also provides a time history of rms heading error and magnetic heading reference error. Prior to the turn, heading errors are essentially bounded by the assumed heading reference error magnitude (1 deg rms). The occurrence of a turn leads to significant calibration of heading error and, therefore, of the heading reference error. The calibration is associated with the combined effect of the heading error and the velocity change in the cross axis on velocity error measurements. Between turns, the heading accuracy degrades due to uncalibrated c gyro bias, white noise drift, etc. This error behavior is bounded by the degradation in the heading reference error calibration associated with the 0.5 h correlation time.

The effect of variations in the wind model parameters on pitch/roll errors is shown in Figs. 5 and 6. In particular, Fig. 5 provides a time history of rms pitch/roll errors with gyro model B and for several wind models; Fig. 6 provides similar results for gyro model C. Some results from these plots are summarized in Table 4.

These results show that, for a fixed wind variance, the rms pitch/roll errors increase as the correlation time decreases. Also, as would be expected, for a fixed wind correlation time pitch/roll errors increase as the wind variance increases. More generally, a review of the data indicated that pitch/roll errors appeared to be related to a wind model figure-of-merit of $2\,\sigma^2/\tau$. It can be shown that the quantity $2\,\sigma^2/\tau$ represents the high-frequency asymptote for the power spectral density of a first-order Markov process. It was then further postulated that the pitch/roll errors in Figs. 5 and 6 were sensitive to the effects of wind variations in some relatively critical high-frequency band. Because of the known dominance of Schuler loop effects in inertial systems, it was considered probable that the critical frequencies for wind disturbances would be in the neighborhood of 4.5 rad/h. This hypothesis was studied further via Figs. 7 and 8. Figure 7 is a plot of the power spectral density for several of the wind models. Despite the wide disparity in wind variance and correlation times, several of the wind models were selected to have similar high-frequency power. Figure 8 is a plot of the steady-state variance of pitch/roll errors vs the wind power spectral density at a specific frequency near 4.5 rad/h. For gyro model C the selected frequency was 6 rad/h; for gyro models A and B, the selected frequency was 4.5 rad/h (as gyro drift decreases, it is expected that the natural frequency of the system would approach Schuler frequency). The uniformity of the plots on Fig. 8 imply that, as postulated, wind power in the region of approximately 4.5-7 rad/h is an important characteristic of this error source in the systems under consideration.

The effect of the gust model was also briefly examined. All previous results were based on the use of a white gust model with an rms magnitude of 6 kt/axis. A computer run was also made using rms gusts of 18 kt/axis. Results are shown in Fig. 9 for wind model II and gyro model B. The data does not indicate that gust magnitude is a critical parameter. The transients after the turns are somewhat higher in the case of the 18 kt/axis gust model, and the initial settling time is extended slightly.

Conclusions

The accuracy performance of a generic ring laser strapdown attitude and heading reference for aircraft has been described in this paper. Results were presented primarily in the form of time histories of computed rms attitude errors. Attitude accuracy was shown to be dependent on both the magnitude of the white noise component of ring laser drift, and on wind variations in the 4.5-7 rad/h frequency range (wavelength $\cong V_{AS}$ n. mi. where V_{AS} is the airspeed in kt). Several sets of gyro drift and wind model parameters were used in the analysis. It was shown for example that, using the baseline wind model, white gyro drift of 0.01 deg/h$^{1/2}$, 0.05 deg/h$^{1/2}$, and 0.15 deg/h$^{1/2}$, would result in steady-state rms pitch/roll errors of 2.0 arc-min, 2.4 arc-min, and 3.7 arc-min, respectively. The transient effect on pitch/roll errors of several (2 g) aircraft turns was also indicated. Heading errors were shown to be bounded by the assumed error in the magnetic heading reference to an rms value of approximately 1 deg. Some temporary improvement in heading error occurs as a result of aircraft turns; such turns are also effective in calibrating airspeed bias errors (to approximately 2 kt rms), and in assisting the calibration of gyro drifts.

The analysis indicates that the postulated ring laser strapdown attitude and heading reference can provide a level of accuracy performance which exceeds typical requirements.[17] Further, only modest ring laser drift performance is required, and this is available in state-of-the-art units.

Use of a fifteen-state Kalman filter was assumed in the analysis. The particular filter structure described in the paper represents a significant reduction from the dimension of the veridicial model for a ring laser strapdown system (usually more than thirty states[9]). Nevertheless, use of an even lower dimension filter may be possible in an actual implementation without seriously degrading accuracy performance. Sensitivity studies would be required to evaluate candidate structures. It is noted, however, that use of a strapdown system implies the availability of a modern state-of-the-art computer. Within the context of such a computer, the computational burden associated with a fifteen-state Kalman filter may be quite acceptable. For example, recent implementation of a fourteen-state Kalman filter in a marine AHRS, using a 2.56 s iteration interval (which is sufficient for A/C applications) required 2200 words of memory and used less than 5% of the available computation time.

It is generally concluded that current ring laser strapdown systems are fully compatible with accuracy, as well as cost, size, reliability and maintainability requirements of an aircraft AHRS.

Acknowledgments

The author wishes to acknowledge helpful discussions with E. Levinson and constructive suggestions by P. Siskind, both of Sperry Gyroscope.

References

[1] Macek, W.M. and McCartney, E.J., "The Ring Laser," *Sperry Engineering Review,* Vol. 19, No. 1, 1966, pp. 8-15.

[2] Killpatrick, J., "The Laser Gyro," *IEEE Spectrum,* Vol. 4, Oct. 1967, pp. 44-55.

[3] Morrison, R.F., Levinson, E., and McAdory, R., "The SLIC-15 Laser Gyro Inertial Guidance System," *Proceedings of the National Aerospace Symposium, Institute of Navigation,* April 1976, pp. 59-68.

[4] Morrison, R.F., Levinson, E., and Bryant, B., "The SLIC-7 Laser Gyro Inertial Guidance System," *Proceedings of the IEEE National Aerospace and Electronic Conference,* May 1977, pp. 1045-1061.

[5] Savage, P.G., "Laser Gyros in Strapdown Inertial Navigation Systems," IEEE Position Location and Navigation Symposium, San Diego, Calif., Nov. 1976.

[6] Pasik, D., Gneses, M., and Taylor, G., "A Ring Laser Gyro Strapdown Inertial Navigation System: Performance Analysis and Test Results," AIAA Paper 75-1095, Boston, Mass., Aug. 1975.

[7] Thomson, K., Schwartz, B., San Giovanni, C., Young, E., and Howie, G., "The Laser Gyro MK 16 Mod 11 Shipboard Stable Element," *Proceedings of the IEEE National Aerospace and Electronics Conference,* May 1978, pp. 204-219.

[8] Levinson, E., "Laser Gyro Strapdown Inertial System Applications," AGARD-LS-95, 1978, pp. 6-1 to 6-48.

[9] San Giovanni, C., "Performance of a Differential Omega-Ring Laser Strapdown Aircraft Navigator," *Proceedings of the IEEE National Aerospace and Electronics Conference,* May 1978, pp. 1031-1043.

[10] Britting, K.R., *Inertial Navigation Systems Analysis,* Wiley-Interscience, New York, 1971.

[11] Reddy, P.B. and Dushman, A., "Development of Long Term Stability Models for Ring Laser Gyros," Electro Optics/Laser Conference, Anaheim, Calif., Oct. 1977.

[12] Donoghue, P.J., "Strapdown Attitude and Heading Reference System," *Proceedings of the IEEE National Aerospace and Electronic Conference,* May 1974, pp. 556-561.

[13] Hemesath, N.B., "The Optimum Complementation of VOR/DME With Air Data," AIAA Paper 69-841, Princeton, N.J., Aug. 1969.

[14] Bryson, A.E. and Bobick, J.C., "Improved Navigation by Combining VOR/DME Information and Air Data," AIAA Paper 72-846, Stanford, Calif., Aug. 1972.

[15] Savage, P.G. and Hartmann, G.L., "Optimum Aiding of Inertial Navigation Systems Using Air Data," AIAA Paper 72-847, Stanford, Calif., Aug. 1972.

[16] Blasingame, B.J., "Optimum Parameters for Automatic Airborne Navigation," MIT Instrumentation Laboratory, Cambridge, Mass., 6398-T-8, 1950.

[17] Strapdown AHRS ARINC Specification No. 705, 1978.